Silver nanorods absorber for passively Q-switched Nd,Gd:CaF_2 laser

Yongjing Wu (吴永静)[1], **Siyuan Pang** (逄思远)[3,4], **Yuqian Zu** (祖玉倩)[1], **Qianqian Peng** (彭倩倩)[1], **Jimin Yang** (杨济民)[1], **Jie Liu** (刘 杰)[1,2,*], **and Liangbi Su** (苏良碧)[3,4]

[1]*Shandong Provincial Key Laboratory of Optics and Photonic Device, School of Physics and Electronics, Shandong Normal University, Jinan 250014, China*

[2]*Institute of Data Science and Technology, Shandong Normal University, Jinan 250014, China*

[3]*Synthetic Single Crystal Research Center, Shanghai Institute of Ceramics, Chinese Academy of Sciences, Shanghai 201800, China*

[4]*Key Laboratory of Transparent and Opto-functional Inorganic Materials, Shanghai Institute of Ceramics, Chinese Academy of Sciences, Shanghai 201800, China*

**Corresponding author: jieliu@sdnu.edu.cn*

Received July 17, 2017; accepted September 4, 2017; posted online December 26, 2017

Using a novel silver nanorods absorber with a localized surface plasmon resonance absorption peak at 1.06 μm, we obtain a diode-pumped passively Q-switched (PQS) Nd,Gd:CaF_2 disordered crystal laser output. Its PQS pulse laser performances are studied comprehensively and systematically in this Letter. The single pulse energy and peak power can be attained to 2.15 μJ and 2.06 W, respectively.

OCIS codes: 140.0140, 140.3380, 140.3480, 140.3540, 160.4236.
doi: 10.3788/COL201816.020015.

Passively Q-switched (PQS) solid-state lasers at 1.06 μm have a wide range of application prospects in scientific research, medical treatment, and even laser cosmetology due to their high photon energy, wide absorption bandwidth, and easy thermal management[1]. Two key factors affect the PQS laser performances, laser materials, and saturable absorbers (SAs). On the one hand, the progress of materials used as SAs has promoted the advancement of pulse lasers. Very recently, when the research boom of two-dimensional materials such as graphene[2–5], transition metal dichalcogenides (MoS_2, WS_2, etc.)[6,7], topological insulators (Bi_2Se_3, Bi_2Te_3, etc.), and black phosphorus (BP) has not yet subsided, metal nanomaterials, one of them, have attracted increasing attention due to their interesting optical properties and application prospects[8–23]. This is because noble metal nanoparticles dispersed in dielectric media exhibit ultrafast nonlinear optical responses around localized surface plasmon resonance (LSPR), resulting in potential applications in SAs[8–10]. Most importantly, the LSPR peak is variable by controlling aspects of the nanomaterials[9–13,15,18–21,23]. Moreover, the large third-order nonlinear and fast response time as a time scale of few picoseconds are also excellent nonnegligible optical properties of metal nanomaterials[13–15,21–23].

Silver nanorods (SNRs), a component of these typical metal nanomaterials, have also played a significant role in photonic device applications, especially as a wideband SA for versatile pulsed lasers[15–17]. A large third-order optical nonlinearity ($\chi^{(3)} \approx 10^{-10}$ esu) of silver nanoparticles dispersed in polyvinyl alcohol/tetraethyl orthosilicate matrix has been obtained using a single-beam Z scan technique[14]. Moreover, in a PQS erbium-doped fiber laser, 2.4 μs pulses were generated containing silver nanoparticle-based SAs[16]. These results indicate the potential and advantages of SNRs as SAs. But at present the application of silver nanomaterials in all solid-state lasers is still relatively rare.

On the other hand, laser materials, as the core and foundation of the development of laser technology, have had a landmark effect on the development of solid-state lasers[24]. Compared with other laser materials, alkaline earth AeF_2 fluoride crystals (Ae: Ca^{2+}, Sr^{2+}, Ba^{2+}, etc.), with the unique advantages of low refractive index and thermal lens effect, spontaneous long fluorescence lifetime, and good thermal stability, have special value applications in the field of solid lasers. Particularly, the $AeF_2 - LnF_3 - NdF_3$ (Ln: Y^{3+}, Lu^{3+}, La^{3+}, Gd^{3+}) disordered crystals have excellent laser outputs[19,25–34]. The addition of non-optically active ions (Y^{3+}, Lu^{3+}, La^{3+}, Gd^{3+}) could effectively relieve the pernicious concentration of quenching, and significantly improve their absorption, emission, fluorescence lifetime properties, and their laser performance[26,27]. Doualan, *et al.* obtained the efficient continuous-wave (CW) laser operation of Nd,Y:CaF_2, and Nd,Lu:CaF_2 crystals, and they demonstrated that co-doping Nd:CaF_2 single crystals with Y^{3+} and Lu^{3+} buffer ions significantly improved their characteristics and their laser performance[26]. Then, Qian *et al.* increased the Nd,Y:CaF_2 CW laser maximum output power to 901 mW[28]. In recent years, extensive researchs on mode-locking lasers based on Nd^{3+}-doped CaF_2 crystals

have been reported[2,30–34], which shows great potential for generating ultra-short pulses. However, the Nd,Gd:CaF_2 crystals' laser performances have not been studied and reported so far.

In this Letter, we combined the unique optical property of SNR absorbers as well as the merit of Nd,Gd:CaF_2 disordered crystals, and demonstrated a diode-pumped PQS Nd,Gd:CaF_2 laser using SNRs-based SAs for the first time, to our knowledge. The shortest pulse width was 1.046 μs, and the corresponding repetition rate and single pulse energy were 53.92 kHz and 2.15 μJ, respectively. Our results reveal the potential of SNRs for pulse generation in the 1.06 μm region. As fast response SAs, SNRs have a promising prospect of application to ultra-short pulse generation.

The SNRs used in our experiment were prepared using a seed-mediated growth method. In the preparation of an SNRs solution, some small-sized gold nanobipyramids solution needed to be prepared as a growth solution. 2 mL of $HAuCl_4$ (0.1 mol/L) solution, 400 μL of $AgNO_3$ (0.01 mol/L) solution, and 800 μL of HCl (0.1 mol/L) solution were dissolved into 40 mL of cetyltrimethylammonium bromide (CTAB) (0.1 mol/L) solution. Then 200 μL of the sample was added to the seed solution and placed in an oven heated at 65 °C for 10 h to form the growth solution. After completing the above work, 5 mL of the growth solution was removed and centrifuged at 6000 r/min for 10 min and then transferred into a 15 mL of cetyltrimethylammonium chloride (CTAC) with the concentration of 0.08 mol/L (about 384 mg in 15 mL). Then 300 μL of $AgNO_3$ (0.01 mol/L) solution and 150 μL of ascorbic acid (0.1 mol/L) solution were added to the mixed solution, and the sample was heated at 65 °C for 4 h. Finally, the solution was transferred to a quartz carrier substrate with a spin-coating method and then followed by slow drying at room temperature to form SNRs SA film. In order to further analyze the morphology and size of the sample, transmission electron microscopy (TEM) was utilized, as shown in Fig. 1. The ultraviolet-visible (UV-Vis) extinction spectra of the SNRs showed a conspicuous SPR absorption peak at around 1066 nm [Fig. 1(b)]. This indicates the possibility of the SNRs as an SA used in pulsed lasers.

A nonlinear optical response property was then carried out on SNRs SA film to confirm its saturable absorption near 1.06 μm. A self-constructed mode-locked Yb:KGW laser (1047 nm wavelength, 12 ps pulse width, 86.6 MHz repetition rate) was used as the seed source. We quoted a model of $T(I) = 1 - \varphi_0 \times \exp(-I/I_{sat}) - \varphi_{ns}$[6] to characterize a nonlinear optical curve [$T(I)$, φ_0, I, I_{sat}, and φ_{ns} correspond to transmission, modulation depth, input optical intensity, saturation optical intensity, and non-saturable loss, respectively]. From the nonlinear absorption curve depicted in Fig. 1(d), the modulation depth, non-saturable loss, and saturation optical intensity were calculated to be 41.1%, 12.4%, and 25.46 mW/cm^2, respectively.

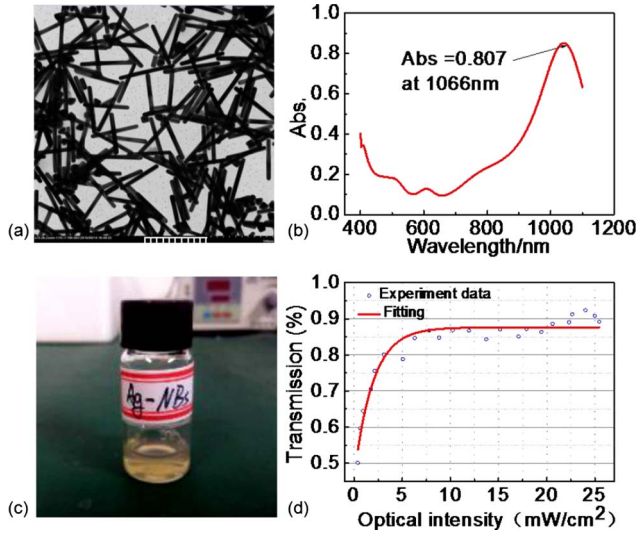

Fig. 1. (a) TEM image of the SNRs SA with a scale bar of 500 nm; (b) the absorption intensity coefficient of the SNRs SA; (c) a photograph of SNRs solution; (d) the nonlinear transmission curve of the SNRs SA.

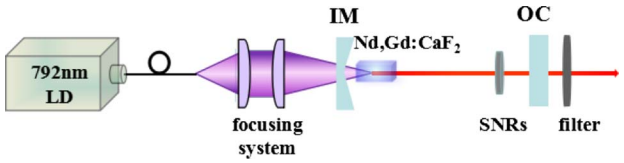

Fig. 2. Schematics of diode-pumped Nd,Gd:CaF_2 lasers in the CW mode and the PQS mode.

The schematic of the diode-pumped Nd,Gd:CaF_2 laser in the CW and PQS regimes is schematically shown in Fig. 2. In order to evaluate the performances of the SNRs SA and ensure TEM_{00} output, we designed a 30 mm long compact concave-plane linear resonator, that ensured that the intrinsic mode size of both the laser crystal and SAs not be considerably affected by the thermal lens effect. The input concave mirror with a 100 mm radius of curvature was high-transmission-coated at 808 nm and high-reflection-coated for the output laser at 1064 nm. A plane mirror with different transmissions (T) of 2% and 3% at 1064 nm were used as an output coupler (OC). The pump source was a fiber-coupled 792 nm diode laser with a core diameter of 105 μm and a numerical aperture of 0.22. Its radiation was coupled into the laser crystal by a 1:2 focusing optical system. An uncoated novel Nd,Gd:CaF_2 crystal with dimensions of 3 mm × 3 mm × 5 mm and doping of 0.5 at.% Nd^{3+} and 5 at.% Gd^{3+} was employed as the gain medium. The laser crystal was wrapped within indium foil and mounted into a water-cooled copper block to dissipate most of the heat. Calculated by the ABCD-matrix method, the laser mode size inside the Nd,Gd:CaF_2 crystal was about 128 μm in radius, which matched well with the pump size.

To characterize laser performances, the output power was measured by a 30A-SH-V1 power meter (made by

Israel) while the laser pulse temporal behavior was recorded by a Tektronix DPO4104 digital oscilloscope (1 GHz bandwidth) and a fast InGaAs photodetector with a rise time less than 175 ps. The emission spectrum was measured by an optical spectrum analyzer from SOL instruments (Model No: MS 3504i) while the beam quality and spatial beam profile (M^2) were gauged by using an M^2 factor analyzer (Spiricon-M^2-200S -USB).

For verifying the feasibility of the resonator design, the CW laser performances were studied first. In the CW regime, when the absorbed pump power was 1.51 W, the average output powers of 496 and 477 mW were generated by using OCs with transmissions of 2% and 3% and corresponding slope efficiencies of 38.1% and 36.2%, respectively. Figure 3 shows the CW average output power versus the absorbed pump power.

In the Q-switched experiment, the concave-plane linear resonator was still used, and the two OCs with transmissions of 2% and 3% were still selected to generate the Q-switched pulse. The laser mode size in the SNRs-based SA was about 80 μm in radius. After inserting the SNRs SA close to OC inside the resonator, stable passively Q-switching started when the absorbed pump powers exceeded the thresholds of 0.49 and 0.55 W for $T = 2\%$ and 3%, respectively. Maximum average output powers of 118 and 116 mW were obtained, and the corresponding slope efficiencies were 12.5% and 12.6%, respectively. The relationship between the average output power and the absorbed pump power was plotted in Fig. 4. It could be seen that the average output power increased almost linearly with the absorbed pump power. At the maximum average output power, we recorded the fluctuation of the Q-switched laser for 40 min, as shown in inset (a) of Fig. 5. The instability of the average output power was ~7.9%, which described the relatively excellent stability of the Q-switched laser. With the increase of the absorbed pump power from the threshold to 1.35 W, the pulse width presented a rapid drop from 1.943 to 1.239 μs for $T = 2\%$, and the pulse width decreased from

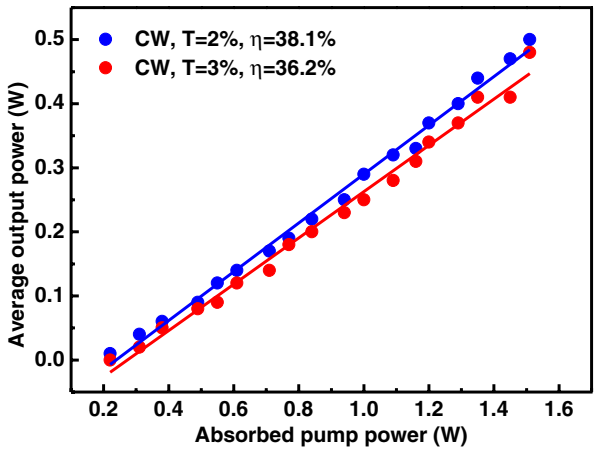

Fig. 3. (Color online) Average output power versus the absorbed pump power for CW.

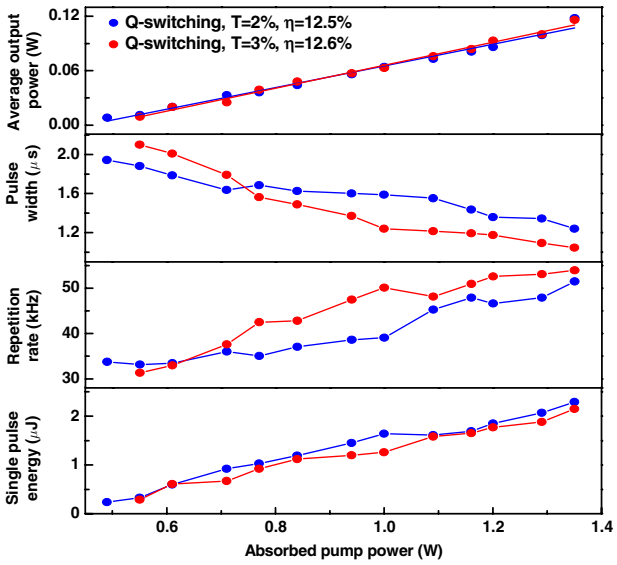

Fig. 4. (Color online) Average output power, pulse width, repetition rate, and single pulse energy of the Q-switched Nd, Gd:CaF_2 laser versus the absorbed pump power.

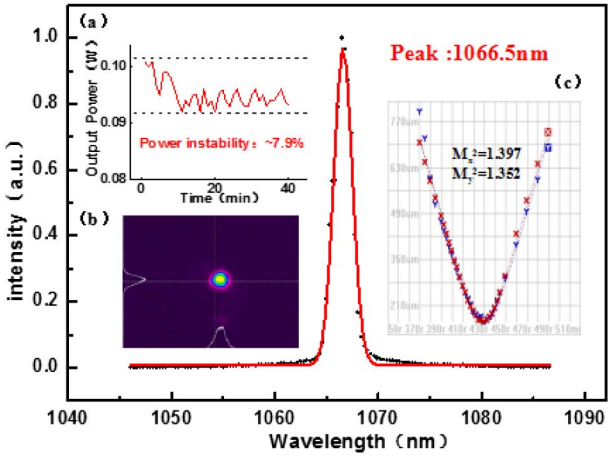

Fig. 5. Laser emission spectrum of the Q-switched pulse trains with $T = 3\%$; (a) the instability of the average output power measured during the 40 min with $T = 3\%$; (b) the beam quality of the Q-switched laser with $T = 3\%$; (c) the spatial beam profile of the Q-switched laser with $T = 3\%$.

2.101 μs to the minimum data of 1.046 μs for $T = 3\%$. When the transmission increased from 2% to 3%, the repetition rate increased while the single pulse energy decreased accordingly. Detailed experimental results are summarized in Table 1.

The Q-switched pulse trains were measured as shown in Fig. 6. The Q-switched pulses began to be unstable since the absorbed pump power exceeded 1.35 W. To exclude the thermal damage of the SNRs SA, the pump power was decreased and then the pulses became stable again. We repeated it for three times. The pulses could always be stabilized again, indicating no damage to the SNRs SA. We think the possible reasons for instability are as follows: (1) there is a thermal agglomeration phenomenon

Table 1. Results of the Q-switched Nd, Gd:CaF_2 Laser Obtained with $T = 2\%$ and 3%

Transmission of the OC	$T = 2\%$	$T = 3\%$
Maximum average output power	118 mW	116 mW
slope efficiency	12.5%	12.6%
Repetition rate	51.48 kHz	53.92 kHz
Shortest pulse width	1.239 μs	1.046 μs
Single pulse energy	2.29 μJ	2.15 μJ
Peak power	1.85 W	2.06 W

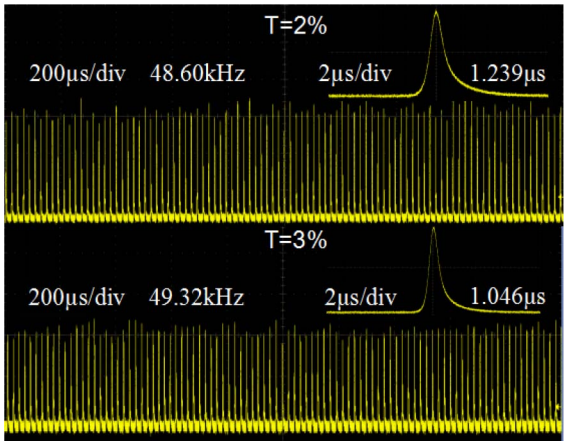

Fig. 6. Typical pulse trains of the Q-switched laser in different time scales

in the nanomaterials that, at higher pump power, causes some variations in the LSPR absorption peak, which makes the modulation unstable; (2) LSPR absorption is a process of resonance absorption, the uneven arrangement of materials will cause the instability of absorption. Further improvements will be made in after work, which will be used to improve SNRs properties of the composite graphene or the installation of an SiO_2 shell and the specific arrangement of SNRs, and ultra-short pulse generation is expected.

After the pulse stabilization, the laser emission spectrum was measured, as shown in Fig. 5. It was obvious that the laser operated at 1066.5 nm, which corresponded to the high-absorption region of the SNRs SA. The illustrations in Fig. 5 show the beam quality and spatial beam profile (M^2) curve fitted with a hyperbolic function. Both the relatively low M^2 value and symmetrical distribution of the spatial distribution in the two-dimensional space demonstrated that the laser was operating with a nearly Gaussian mode.

In conclusion, we demonstrate a diode-pumped PQS Nd,Gd:CaF_2 laser with SNRs-based SA. A stable Q-switched laser with the shortest pulse duration of 1.046 μs at the maximum repetition rate of 53.92 kHz is obtained, which is narrower than the outputs of the PQS erbium-doped fiber laser based on silver nanoparticles SA and the PQS laser based on gold nanobipyramids SA[16,19]. The corresponding maximum average output power, single pulse energy, and peak power are 116 mW, 2.15 μJ, and 2.06 W, respectively. The results indicate the potential of SNRs as SAs for diode-pumped solid-state lasers. Considering the large third-order optical nonlinearity intrinsic to metal nanoparticles, as the SNRs parameters and the resonator design are further optimized, CW mode-locked operation might be feasible.

This work was supported by the National Natural Science Foundation of China under Grant Nos. 61475089, 61422511, 61635012, and 51432007.

References

1. N. A. M. Taib, N. Bidin, H. Haris, N. N. Adnan, M. F. S. Ahmad, and S. W. Harun, Opt. Laser Technol. **79**, 193 (2016).
2. H. T. Zhu, J. Liu, S. Z. Jiang, S. C. Xu, L. B. Su, D. P. Jiang, X. B. Qian, and J. Xu, Opt. Laser Technol. **75**, 83 (2015).
3. Y. F. Song, L. Li, H. Zhang, D. Y. Shen, D. Y. Tang, and K. P. Loh, Opt. Express **21**, 10010 (2013).
4. H. Zhang, D. Y. Tang, R. J. Knize, L. M. Zhao, Q. L. Bao, and K. P. Loh, Appl. Phys. Lett. **96**, 111112 (2010).
5. W. Cai, S. Z. Jiang, S. C. Xu, Y. Q. Li, J. Liu, C. Li, L. H. Zheng, L. B. Su, and J. Xu, Opt. Laser Technol. **65**, 1 (2015).
6. J. Lu, X. Zou, C. Li, W. Li, Z. Liu, Y. Liu, and Y. Leng, Chin. Opt. Lett. **15**, 041401 (2017).
7. Y. Z. Huang, Z. Q. Luo, Y. Y. Li, M. Zhong, B. Xu, K. J. Che, H. Y. Xu, Z. P. Cai, J. Peng, and J. Weng, Opt. Express **22**, 25258 (2014).
8. K. F. MacDonald, Z. L. Samson, M. I. Stockman, and N. I. Zheludev, Nat. Photon. **3**, 55 (2009).
9. M. Kauranen and A. V. Zayats, Nat. Photonics **6**, 737 (2012).
10. S. M. Hamid and M. A. Oskuei, Chin. Opt. Lett. **12**, 031601 (2014).
11. X. Liu, T. J. He, F. C. Liu, and D. M. Chen, Chin. J. Chem. Phys. **18**, 81 (2005).
12. R. Wang, L. Y. Pan, X. D. Xia, D. A. Han, J. Qi, and H. Yang, Chem. J. Chin. Univ. **33**, 149 (2012).
13. H. M. Gong, H. W. Dai, J. B. Han, K. Zhang, Y. B. Han, and Z. L. Huang, Opt. Mater. Express **5**, 2648 (2015).
14. V. Singh and P. Aghamkar, Appl. Phys. Lett. **104**, 111112 (2014).
15. F. Chen, J. Cheng, S. Dai, Z. Xu, W. Ji, R. Tan, and Q. Zhang, Opt. Express **22**, 3438 (2014).
16. H. Guo, M. Feng, F. Song, H. Y. Li, A. B. Ren, X. K. Wei, Y. G. Li, X. X. Xu, and J. G. Tian, IEEE Photon. Technol. Lett. **28**, 135 (2015).
17. D. A. Glubokov, V. V. Sychev, A. S. Mikhailov, A. E. Korolkov, D. A. Chubich, B. I. Shapiro, and A. G. Vitukhnovskii, Quantum Electron. **44**, 314 (2014).
18. Z. Z. Chu, H. N. Zhang, Y. J. Wu, and J. Liu, Opt. Commun. **406**, 209 (2018).
19. F. Zhang, H. N. Zhang, D. H. Liu, J. Liu, F. K. Ma, D. P. Jiang, S. Y. Pang, L. B. Su, and J. Xu, Chin. Phys. B **26**, 024205 (2017).
20. Z. Kang, Q. Li, X. J. Gao, L. Zhang, Z. X. Jia, Y. Feng, G. S. Qin, and W. P. Qin, Laser Phys. Lett. **11**, 035102 (2014).
21. X. Wang, N. Zhao, H. Liu, R. Tang, Y. Zhu, J. Xue, Z. Luo, A. Luo, and W. Xu, Chin. Opt. Lett. **13**, 081401 (2015).
22. D. D. Wu, J. Peng, Z. P. Cai, J. Weng, Z. Q. Luo, N. Chen, and H. Y. Xu, Opt. Express **23**, 24071 (2015).
23. X. D. Wang, A. P. Luo, H. Liu, N. Zhao, M. Liu, Y. F. Zhu, J. P. Xue, Z. C. Luo, and W. C. Xu, Opt. Express **23**, 22602 (2015).

24. A. H. Wu, J. Xu, H. B. Chen, and M. L. Shi, Laser Infrared **39**, 8 (2009).
25. J. Liu, M. W. Fan, L. B. Su, D. P. Jiang, F. K. Ma, Q. Zhang, and J. Xu, Laser Phys **24**, 035802 (2014).
26. J. L. Doualan, L. B. Su, G. Brasse, A. Benayad, V. Ménard, Y. Y. Zhan, A. Braud, P. Camy, J. Xu, and R. Moncorgé, J. Opt. Soc. Am. B **30**, 3018 (2013).
27. L. B. Su, Q. G. Wang, H. J. Li, G. Brasse, P. Camy, J. L. Doualan, A. Braud, R. Moncorgé, Y. Y. Zhan, L. H. Zheng, X. B. Qian, and J. Xu, Laser Phys. Lett. **10**, 035804 (2013).
28. Q. Zhang, L. Su, D. Jiang, F. Ma, Z. Qin, G. Xie, J. Zheng, Q. Deng, W. Zheng, L. Qian, and J. Xu, Chin. Opt. Lett. **13**, 071402 (2015).
29. C. Li, M. W. Fan, J. Liu, L. B. Su, D. P. Jiang, X. B. Qian, and J. Xu, Opt. Laser Technol. **69**, 140 (2015).
30. J. F. Zhu, L. J. Zhang, Z. Y. Gao, J. L. Wang, Z. H. Wang, L. B. Su, L. H. Zheng, J. Y. Wang, J. Xu, and Z. Y. Wei, Laser Phys. Lett. **12**, 035801 (2015).
31. Z. P. Qin, G. Q. Xie, J. Ma, W. Y. Ge, P. Yuan, L. J. Qian, L. B. Su, D. P. Jiang, F. K. Ma, Q. Zhang, Y. X. Cao, and J. Xu, Opt. Lett. **39**, 1737 (2014).
32. L. Wei, H. N. Han, W. L. Tian, J. X. Liu, Z. H. Wang, Z. Zhu, Y. L. Jia, L. B. Su, J. Xu, and Z. Y. Wei, Appl. Phys. Express **7**, 092704 (2014).
33. F. Zhang, X. W. Fan, J. Liu, F. K. Ma, D. P. Jiang, S. Y. Pang, L. B. Su, and J. Xu, Opt. Mater. Express **6**, 1513 (2016).
34. Z. P. Qin, Q. Zhen, G. Q. Xie, Y. Peng, J. G. Ma, L. J. Qian, D. P. Jiang, F. K. Ma, F. Tang, and L. B. Su, IEEE Photon. J. **9**, 1502007 (2017).